# Inter-model variations in projected precipitation change over the North Atlantic: Sea surface temperature effect

Shang-Min LONG[1, 2*] and Shang-Ping XIE[1, 2]

*[1]Physical Oceanography Laboratory/Qingdao Collaborative Innovation Center of Marine Science and Technology, Ocean-Atmosphere Interaction and Climate Laboratory, Ocean University of China, Qingdao, China*

*[2] Scripps Institution of Oceanography, University of California at San Diego, La Jolla, California, USA*

*Corresponding author: Shang-Min Long, email: smlong4861@gmail.com

## ABSTRACT

Inter-model variations in future precipitation projection in the North Atlantic are studied using 23 state-of-art models from Phase 5 of the Coupled Model Intercomparison Project. Model uncertainty in annual-mean rainfall change is locally enhanced along the Gulf Stream. The moisture budget analysis reveals that much of the model uncertainty in rainfall change can be traced back to the discrepancies in surface evaporation change and transient eddy effect among models. Results of the inter-model Singular Value Decomposition (SVD) analysis show that inter-model variations in local sea surface temperature (SST) pattern exert a strong control over the spread of rainfall projection among models through the modulation of evaporation change. The first three SVD modes explain more than 60% of the inter-model variance of rainfall projection and show distinct SST patterns with mode-water-induced banded structures, reduced subpolar warming due to ocean dynamical cooling and the Gulf Stream shift, respectively.

## 1. Introduction

Precipitation change under global warming is of great importance for society. Achieving reliable projection of regional rainfall change remains a great challenge for climate science since the sign and amplitude of precipitation change vary spatially [Ma and Xie, 2013]. Uncertainty in future rainfall projection mainly derives from three sources: radiative forcing, model uncertainty and internal variability. Among these three sources, model uncertainty is dominant specifically for longer-term projections [Hawkins and Sutton, 2011]. Model uncertainty in rainfall projection remains large in Phase 5 of the Coupled Model Intercomparison Project (CMIP5) [Taylor et al., 2012], similar to that in CMIP3 [Knutti and Sedlacek, 2013]. It is therefore essential to understand the physical mechanism for the model uncertainty.

In the tropics, precipitation changes mainly follow the sea surface temperature (SST) warming pattern [Xie et al., 2010], as a result of the offset between the wet-get-wetter pattern and tropical circulation slowdown [Seager et al., 2010; Chadwick et al., 2013]. The SST warming pattern effect is apparent in El Niño-induced atmospheric anomalies both in the tropics and extratropics [Zhou et al., 2014]. Furthermore, the inter-model spread of SST warming pattern is important for both the inter-model divergence of tropical precipitation change and circulation change [Ma and Xie, 2013].

Different from the tropical ocean where the mean-circulation-induced convergence accounts for most of the precipitation distribution, rainfall in the midlatitudes is more complicated, involving weather phenomena, strong influence of the SST front and large-scale moisture advection. Transient eddies are important for precipitation, especially along storm tracks [Hoskins and Valdes, 1990] in the boreal winter. A reduction in the

Meridional Overturning Circulation is associated with a substantial SST cooling over the North Atlantic [Rahmstorf et al., 2015]. This SST pattern increases the meridional SST gradient and baroclinic instability and hence strengthens the local storm track (Woollings et al. 2012). The Gulf Stream transports a large amount of heat to the midlatitudes, forming a long and narrow SST front that anchors a band of heavy rainfall and strong evaporation [Yu, 2007]. The SST front effect is also apparent on synoptic eddies over the North Atlantic [Kwon and Joyce, 2013]. The warm water transported by the Gulf Stream from the tropics supplies much of the water vapor for precipitation via evaporation, resulting in a close relationship between precipitation and evaporation in space. Large-scale moisture advection peaks in the winter, dries the subtropical North Atlantic and moistens the midlatitudes across the horizontal humidity gradient [Seager et al., 2010]. Furthermore, ocean heat transport associated with mode water dynamics [Xie et al., 2010; Xie et al., 2011; Xu et al., 2012] is important for the formation of the midlatitudes SST warming pattern over the North Pacific, forming banded structures in the subtropics [Xie et al., 2010; Long et al., 2014]. Exratropical precipitation change is very similar between Atmospheric General Circulation Model (AGCM) simulations forced with spatially uniform and patterned SST warming [He et al., 2014]. The multi-model ensemble-mean SST warming pattern they used under-estimates the spatial variations, especially over the extratropical North Atlantic where the inter-model differences in SST climatology and warming pattern are large (Fig. 1c). We show that the inter-model spread in SST pattern explains much of the inter-model variations in precipitation change.

The present study examines the sources and mechanism of inter-model spread in precipitation projection in the North Atlantic, based on 23 CMIP5 model projections

(Table S1 in the supporting information). We show that model uncertainty in annual-mean rainfall change is locally enhanced along the Gulf Stream. Our moisture budget analysis reveals that the uncertainty mainly originates from the inter-model discrepancies in evaporation change and transient eddy effect. This is different from the tropical ocean case where the changes in mean convergence dominate the spread of rainfall change among models. The effect of local SST warming pattern on model uncertainty in rainfall projection is examined with the inter-model Singular Value Decomposition (SVD) analyses.

The rest of the paper is organized as follows. Section 2 describes the data and methods. Section 3 discusses the sources of model uncertainty in annual-mean precipitation projection. Section 4 investigates the role of local SST change in the discrepancy of annual-mean rainfall change among models and extends the analysis to the boreal winter and boreal summer. Section 5 is a summary.

## 2. Data and Methods

The monthly outputs of preindustrial control (piControl) runs, historical simulations (1850-2005) and Representative Concentration Pathway 4.5 (RCP4.5, 2006-2100) runs in 23 CMIP5 models are analyzed. Future climate change (denote as $\delta/\Delta$) is calculated by subtracting the 50-year mean of 1950-1999 (present climatology) in historical simulation from the 2050-2099 mean (RCP4.5 climatology) in the RCP4.5 run and then normalized by the domain mean (80°W-0°, 20°N-60°N) SST warming in each model to highlight the uncertainty in spatial pattern. Internal variability causes uncertainty in projections of regional climate in the midlatitudes [Deser et al., 2012] and contributes to the total model uncertainty. To evaluate the contribution from internal variability, we first calculate 100-

year rainfall trends for every 50 years based on the 50-year running mean time series of piControl run in each model. Then one trend is randomly selected per model and used to calculate the inter-model standard deviation at each grid point. To obtain robust results, we repeat the random selection and standard deviation calculation 100 times and average all the resultant inter-model standard deviations as the model uncertainty induced by internal variability. All model outputs are interpolated onto a common grid of 2.5° latitude × 2.5° longitude. Only one member run (r1i1p1) per model is analyzed to ensure equal weight for each model. Note that the near-surface specific humidity in 2 models and wind speed in 4 models are not available (see Table S1).

The moisture budget derived from the water vapor conservation equation for monthly time average is [Trenberth and Guillemot, 1995; Seager et al., 2010]:

$$\rho_w g(P-E) = -\int_0^{p_s} (\boldsymbol{u}\cdot\nabla q)dp - \int_0^{p_s} (q\nabla\cdot\boldsymbol{u})dp + residual. \qquad (1)$$

Here P is precipitation, E is evaporation, $\rho_w$ is the density of water, q is specific humidity, $\boldsymbol{u}$ is the horizontal vector wind, p is pressure and the subscript s denotes the surface value. The first term on the right-hand is moisture advection by the monthly mean circulation and the second term is the wind convergence term and the residual is largely due to transient eddy effect.

For climate change, we neglect the small nonlinear terms. Equation (1) can be approximated as:

$$\delta P = \delta E - \frac{1}{\rho_w g}\int_0^{p_s}(\boldsymbol{u}\cdot\nabla\delta q)dp - \frac{1}{\rho_w g}\int_0^{p_s}(\delta\boldsymbol{u}\cdot\nabla q)dp - \frac{1}{\rho_w g}\int_0^{p_s}(\delta q\nabla\cdot\boldsymbol{u})dp - \frac{1}{\rho_w g}\int_0^{p_s}(q\nabla\cdot\delta\boldsymbol{u})dp + residual. \quad (2)$$

Terms involving $\delta q$ are referred to as themodynamical contribution, and terms involving $\delta\boldsymbol{u}$ as dynamical contribution [Seager et al., 2010]. Thus the thermodynamical and dynamical components each have two subcomponents due to moisture advection and wind convergence. The moisture budget analysis is an effective way to diagnose causes of precipitation change, and will be applied to the analysis of inter-model variations in this study.

Change in evaporation involves either change in sea-air humidity gradient (denote as dq), or wind speed, or both [Yu, 2007]. Sea-air humidity gradient is defined as the difference between the saturation specific humidity at the sea surface temperature ($q_s$) and the near-surface (at the 2m height in the models) atmospheric specific humidity ($q_a$): $dq = q_s - q_a$.

## 3. Sources of model uncertainty in precipitation change

Figure 1 displays model uncertainty, estimated as the inter-model standard deviation, of precipitation change, contribution from internal variability, SST change and the six components of rainfall change in Eq. (2) in the North Atlantic. The tropics are included for comparison. There are two distinct regions with maximum uncertainty in rainfall projection: an extratropical band extending from the subtropics to high latitudes, and the tropical Atlantic (Figure 1a). Model uncertainty is generally larger than the ensemble-mean change, especially over regions where the agreement on the sign of rainfall change among model is low (Fig. S1). In deed, the domain mean (80°W-0°, 20°N-60°N, ocean only) of the signal-to-noise ratio, defined as the absolute value of the ensemble-mean divided by the inter-model standard deviation ($\frac{|\Delta P|}{\sigma(\Delta P')}$), of annual-mean rainfall change is only 0.63. Here Δ denotes climate change, the prime the deviation from the ensemble-mean change, and $\sigma$ the standard deviation. For the model uncertainty in projected rainfall change over 100 years in RCP4.5 run, the contribution from internal variability is small (Figure 1b).

In the extratropical North Atlantic, the discrepancy in evaporation change among models associated with large inter-model difference in SST warming is important (Figures 1c, d). The SST warming pattern can efficiently affect the sea-air humidity gradient and wind speed change, especially along the Gulf Stream where evaporation is large (Yu, 2007). The second major source of uncertainty is the inter-model spread in transient eddy effect (Figure 1i), which is important for midlatitudes rainfall and related to SST gradient [Woollings et al., 2012]. The inter-model variations in the thermodynamical and dynamical contributions in Eq. (2) are relatively small and mainly origin from the differences in simulating the large horizontal humidity gradient and the Gulf Stream-induced wind convergence (Figures 1e-h). In the tropical Atlantic, by contrast, model uncertainty in rainfall projection is dominated by the dynamical contribution due to wind convergence (Figure 1g). Thus mechanisms for inter-model spread in precipitation projection are totally different between the tropical and extratropical North Atlantic. Here we focus on the extratropical North Atlantic and will discuss the model uncertainty in the tropics elsewhere.

## 4. Effect of local SST effect on precipitation change

We examine the dominant pattern of inter-model co-variability by the SVD method. Figure 2 shows the first three inter-model SVD modes between $\Delta P'$ and $\Delta SST'$ and the regressions of $\Delta E'$, sea-air humidity gradient change and scalar surface wind speed change onto the PCs of $\Delta SST'$.

The first SVD mode (SVD1) of $\Delta P'$ displays banded structures that tilt in the northeast-southwest direction, associated with a banded SST pattern that resembles the SST warming pattern due to mode water change [Xie et al., 2010]. The spatial correlation between $\Delta P'$ and $\Delta SST'$ patterns is 0.79 for the SVD1, indicating physical significance of the covariance. Indeed, the regressed evaporation pattern closely resembles the $\Delta P'$ pattern with a spatial correlation of 0.89, suggestive of a robust relationship between the SST-induced evaporation change and the rainfall projection.

To verify the role of mode water in the formation of the banded SST pattern in the SVD1 mode, we select a specific model (ACCESS1-0), in which the banded structures of $\Delta P'$, $\Delta SST'$ and $\Delta E'$ are pronounced (Figure 3). The spatial correlations of $\Delta P$ with $\Delta SST$ and $\Delta E$ are high in this model (Figures 3a,b) at 0.63 and 0.74, respectively. Changes in sea-air humidity gradient and surface wind speed display similar patterns to the evaporation change, confirming their effect on evaporation. Furthermore, the upper ocean current displays banded structures, with warm (cold) advection from lower (higher) latitudes causing enhanced (reduced) SST warming (Figure 3a).

This upper ocean current change is tightly coupled with the mode water change [Xie et al., 2011; Xu et al., 2012]. The mode water is a thick layer of water with vertically uniform properties, whose change affects the upper ocean pycnocline and circulation [Kobashi and Kubokawa, 2012]. In the North Atlantic, the subtropical mode water mainly forms in the deep winter mixed layer south of the Gulf Stream [McCartney and Talley, 1982; Hanawa and Talley, 2001]. Figures 3c,d show the vertical sections along 42°W of seawater temperature and zonal current. The mode water of vertical uniform temperature appears in 25°-40°N at depths of 200-400m in the present climatology

(Figure 3c, black contours). It forces the upper thermocline (e.g. the 20°C isotherm) to shoal and generates eastward (westward) zonal current band at its north (south) side (Figure 3d) via thermal wind relation. Note that the strong zonal velocity in 40°N-45°N is part of the large-scale gyre unrelated to the mode-water. In the RCP4.5 climatology (Figure 3c, white contours), the mode water shifts northward, as indicated by the bulge of the 18°C isotherm. The northward shift of mode water causes the upper thermocline to deepen (shoal) to the south (north). This results in a cooling around 35°N in the upper ocean, which is quite unusual against the background of thermodynamic warming. The subsurface causes an anomalous eastward (westward) current to the south (north) (Figures 3a,d). Note that the zonal velocity change is negligible below 600m, suggesting that the changes in large-scale gyre circulation are secondary.

The SVD2 mode shows negative rainfall change corresponding to the substantially reduced SST warming over the subpolar region and short banded structures south of 45°N (Figure 2b). This negative subpolar SST indicates the importance of the ocean dynamical cooling effect associated with the deep-water formation [Manabe et al., 1990; Long et al., 2014]. The SVD3 mode represents a Gulf Stream shift pattern in the inter-model variations of SST (Figure 2c), as revealed by the two neighboring elongated bands extending from the west to the east with opposite signs.

The spatial correlations of $\Delta P'$ pattern with $\Delta SST'$ pattern and the regressed $\Delta E'$ pattern are prominent in all the first three SVD modes (see Table S2). This happens because variables important to the evaporation, like sea-air humidity difference [Cayan, 1992; Zhang and Mcphaden, 1995; Yu, 2007] and surface wind speed [Chelton and Xie, 2010], are all influenced by the SST. The effect of the SST pattern on changes in sea-air humidity gradient and surface wind speed are clear in the North Atlantic (Figures 2d-f), positively correlated with the SST pattern. This positive correlation between SST and surface wind speed patterns indicates the ocean warming drives the wind response [Chelton and Xie, 2010]. Besides, the effects of sea-air humidity gradient and surface wind speed reinforce each other on evaporation. Consequently, inter-model variations in SST warming pattern exert a strong control on the inter-model divergence of precipitation change over the extratropical North Atlantic.

The first three modes account for 61% and 71% of the inter-model variance of $\Delta P'$ and $\Delta SST'$, respectively. We also examined the next 7 SVD modes of $\Delta P'$ and $\Delta SST'$ and found that positive relationship between them is robust in almost all modes (Table S2). This further confirms the role of the inter-model spread of local SST in explaining the model uncertainty in precipitation change.

Precipitation in the North Atlantic has a robust seasonal cycle with the peak in the boreal winter (DJF, December-January-February), associated with similar seasonal variability in evaporation [Yu, 2007]. The inter-model standard deviations of $\Delta P'$, $\Delta E'$ and $\Delta SST'$ are much larger in DJF than JJA (June-July-August) (Figure 4). This indicates that much of the inter-model discrepancy of precipitation change develops in the boreal winter. The spatial distributions of inter-model standard deviations in these three variables are very similar in DJF but substantially different in JJA. In JJA, for example, the inter-model standard deviation of $\Delta P'$ is largest off the U.S. east coast but the maximum of the inter-model standard deviations of $\Delta E'$ and $\Delta SST'$ are found far apart to the northeast in the subpolar region (Figures 4d-f). Furthermore, spatial correlation between patterns of $\Delta P'$ and $\Delta SST'$ in the inter-model SVD analysis is high in DJF but low in JJA (Table S2), illustrating that the local SST effect on rainfall change reaches the maximum in the boreal winter. All the above analyses highlight the importance of improving simulations of SST warming pattern, especially in the boreal winter, for reliable precipitation projection.

## 5. Summary

We have investigated the model uncertainty in precipitation projection under global warming and the local SST effect in the North Atlantic in CMIP5 models. For both annual- and seasonal-mean precipitation changes, inter-model spread is generally larger than the ensemble-mean change (Fig. S1), lowering the confidence in both the sign and magnitude of the future projections. Model uncertainty in rainfall projection is large along the Gulf Stream. Similar enhanced inter-model variability in precipitation change is also found in other west boundary current regions, such as the Kuroshio and its extension and the Agulhas Current (not shown), where local evaporation supplies much of the water vapor for precipitation and latent heating for transient eddy activity. This occurs because local SST effects of sea-air humidity gradient and surface wind speed reinforce each other on evaporation changes in west boundary current regions [Yu, 2007; Chelton and Xie, 2010]. As a result, inter-model variations in local SST change account for much of the inter-model difference of precipitation change. The inter-model SVD analysis between changes in precipitation and SST confirms this result. The local SST change effect on the inter-model diversity of precipitation change spreads in a large number of inter-model SVD modes, indicating the difficulty for extracting the local SST influence with a few leading modes.

We performed moisture budget analysis for model uncertainty in rainfall projection. The inter-model discrepancies in evaporation change and transient eddy effect are two dominant sources in the extratropical North Atlantic. Further analyses show that model uncertainty in precipitation and evaporation changes reach the maximum in DJF when the effect of the inter-model variations in SST change is the strongest. The effect of the mean atmospheric circulation change is dominant for the model uncertainty in rainfall change in the tropical ocean, but is secondary in the extratropical North Atlantic.

Our results imply that reducing the inter-model spread in SST change, especially in the boreal winter, can greatly improve the consistency of precipitation projection among models. Ocean dynamics is essential in the formation of the SST warming pattern in the midlatitudes, including mode-water-induced banded structures and the reduced subpolar warming over the deep-water formation region. Work is needed to improve the understanding of key physical processes towards greater inter-model consistency in SST warming pattern.

## Acknowledgements

We acknowledge the WCRP Working Group on Coupled Modeling, which is responsible for CMIP, and the climate modeling groups (Table S1) for producing and making available their model outputs. All data were downloaded from http://pcmdi9.llnl.gov/. We wish to thank W. Liu and Q. Liu for helpful discussions and anonymous reviews for constructive comments. This work is supported by the National Basic Research Program of China (2012CB955602), NSFC-Shandong Joint Fund for Marine Science Research Centers (U1406401) and the China Scholarship Council (201406330004).

# References

Cayan, D. R. (1992), Latent and sensible heat-flux anomalies over the northern oceans - the connection to monthly atmospheric circulation, *J. Clim.*, **5**(4), 354-369.

Chadwick, R., I. Boutle and G. Martin (2013), Spatial patterns of precipitation change in CMIP5: Why the rich do not get richer in the tropics, *J. Clim.*, **26**(11), 3803-3822.

Chelton, D. B. and S. -P. Xie (2010), Coupled ocean-atmosphere interaction at oceanic mesoscales. *Oceanography*, **23**(4), 52-69.

Deser, C., A. Phillips, V. Bourdette and H. Teng (2012), Uncertainty in climate change projections: The role of internal variability, *Clim. Dyn.*, **38**(3-4), 527-546.

Hanawa, K. and L. D. Talley (2001). Mode Waters, in *Ocean Circulation and Climate*, edited by G. Siedler, J. Church, and J. Gould, pp. 373-386, Academic Press, San Diego, Calif.

Hawkins, E. and R. Sutton (2011), The potential to narrow uncertainty in projections of regional precipitation change, *Clim. Dyn.*, **37**(1-2), 407-418.

Hoskins, B. J. and P. J. Valdes (1990), On the existence of storm-tracks, *J. Atmos. Sci.*, **47**(15), 1854-1864.

Knutti, R. and J. Sedlacek (2013), Robustness and uncertainties in the new CMIP5 climate model projections, *Nat. Clim. Change*, **3**(4), 369-373.

Kobashi, F. and A. Kubokawa (2012), Review on North Pacific subtropical countercurrents and subtropical fronts: Role of mode waters in ocean circulation and climate, *J. Oceanogr.*, **68**(1), 21-43.

Kwon, Y. O. and Joyce, T. M. (2013), Northern Hemisphere winter atmospheric transient eddy heat fluxes and the Gulf Stream and Kuroshio–Oyashio Extension variability. *J. Clim.,* 26(24), 9839-9859.

Long, S.-M., S.-P. Xie, X.-T. Zheng and Q. Liu (2014), Fast and slow responses to global warming: Sea surface temperature and precipitation patterns, *J. Clim.*, **27**(1), 285-299.

Ma, J. and S.-P. Xie (2013), Regional patterns of sea surface temperature change: A source of uncertainty in future projections of precipitation and atmospheric circulation, *J. Clim.*, **26**(8), 2482-2501.

Manabe, S., K. Bryan and M. J. Spelman (1990), Transient-response of a global ocean atmosphere model to a doubling of atmospheric carbon-dioxide, *J. Phys. Oceanogr.*, **20**(5), 722-749.

McCartney, M. S., and L. D., Talley (1982), The subpolar mode water of the North Atlantic Ocean, *J. Phys. Oceanogr.*, **12**(11), 1169-1188.

Seager, R., N. Naik and G. A. Vecchi (2010), Thermodynamic and dynamic mechanisms for large-scale changes in the hydrological cycle in response to global warming, *J. Clim.*, **23**(17), 4651-4668.

Taylor, K. E., R. J. Stouffer and G. A. Meehl (2012), An overview of CMIP5 and the experiment design, *Bull. Am. Meteorol. Soc.*, **93**(4), 485-498.

Trenberth, K. E. and C. J. Guillemot (1995), Evaluation of the global atmospheric moisture budget as seen from analyses, *J. Clim.*, **8**(9), 2255-2272.

Woollings, T., J. M. Gregory, J. G. Pinto, M. Reyers and D. J. Brayshaw (2012), Response of the North Atlantic storm track to climate change shaped by ocean-atmosphere coupling, *Nat. Geosci.*, **5**(5), 313-317.

Xie, S.-P., C. Deser, G. A. Vecchi, J. Ma, H. Teng and A. T. Wittenberg (2010), Global warming pattern formation: Sea surface temperature and rainfall, *J. Clim.*, **23**(4), 966-986.

Xie, S.-P., L. X. Xu, Q. Liu and F. Kobashi (2011), Dynamical role of mode water ventilation in decadal variability in the central subtropical gyre of the North Pacific, *J. Clim.*, **24**(4), 1212-1225.

Xu, L., S.-P. Xie and Q. Liu (2012), Mode water ventilation and subtropical countercurrent over the North Pacific in CMIP5 simulations and future projections, *J. Geophys. Res. Oceans*, **117**, C12009, doi:10.1029/2012JC008377.

Yu, L. (2007), Global variations in oceanic evaporation (1958-2005): The role of the changing wind speed, *J. Clim.*, **20**(21), 5376-5390.

Zhang, G. J. and M. J. Mcphaden (1995), The relationship between sea-surface temperature and latent-heat flux in the equatorial Pacific, *J. Clim.*, **8**(3), 589-605.

Zhou, Z.-Q., S.-P. Xie, X.-T. Zheng, Q. Liu and H. Wang (2014), Global warming-induced changes in El Nino teleconnections over the North Pacific and North America, *J. Clim.*, **27**(24), 9050-9064.

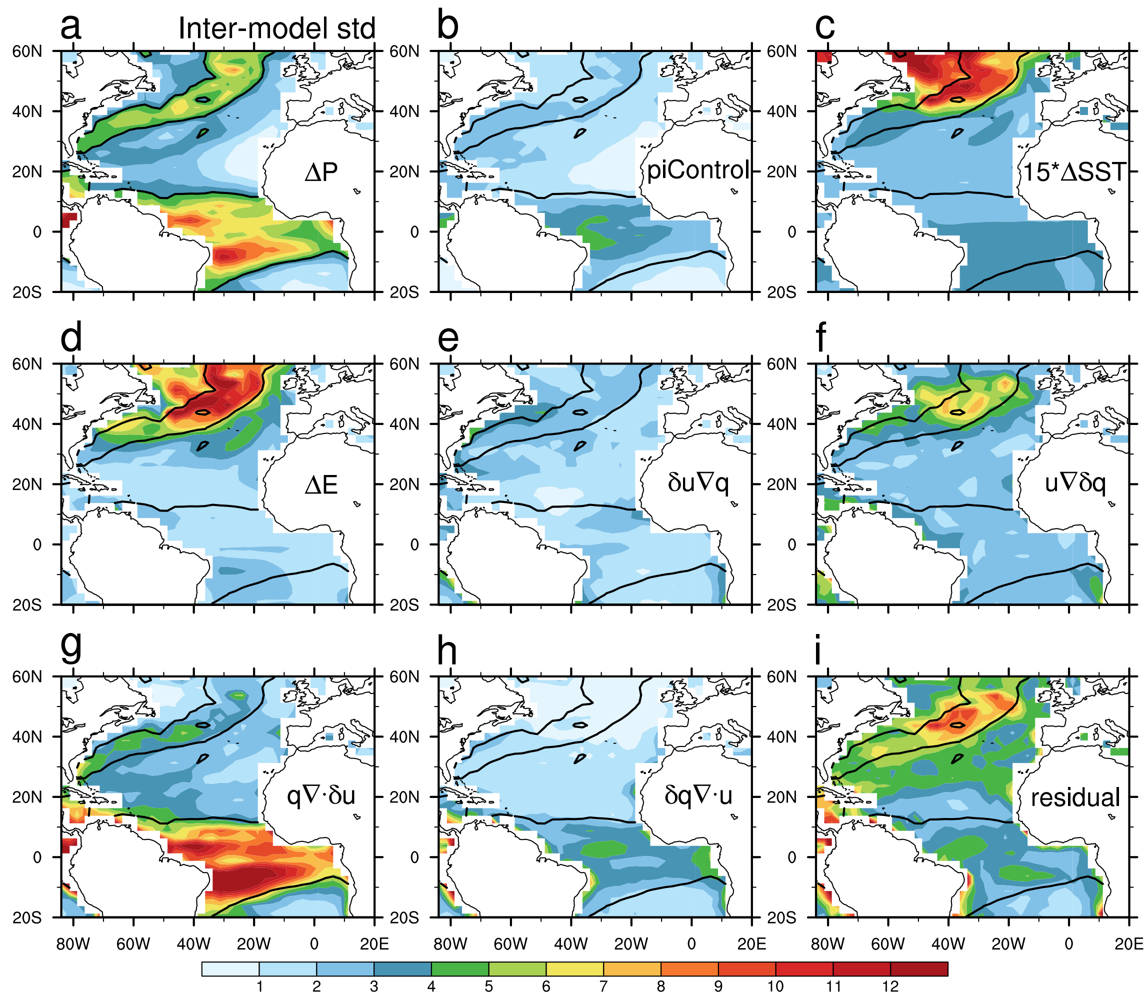


**Fig. 1.** Inter-model standard deviation of (a) precipitation change ($\Delta P$, mm/month), (b) contribution from internal variability, (c) SST change ($\Delta$SST, °C), (d) evaporation change ($\Delta E$), (e) dynamical contribution (with change in mean circulation) due to moisture advection, (f) thermodynamical contribution (with change in specific humidity) due to moisture advection, (g) dynamical contribution due to wind convergence, (h) thermodynamical contribution due to wind convergence, and (i) residual. Black contours indicate value at 4 mm/month in panel (a). All results are normalized by the domain mean (80°W-0°, 20°N-60°N) SST warming. Note that $\Delta$SST is multiplied by a factor of 15 for display.

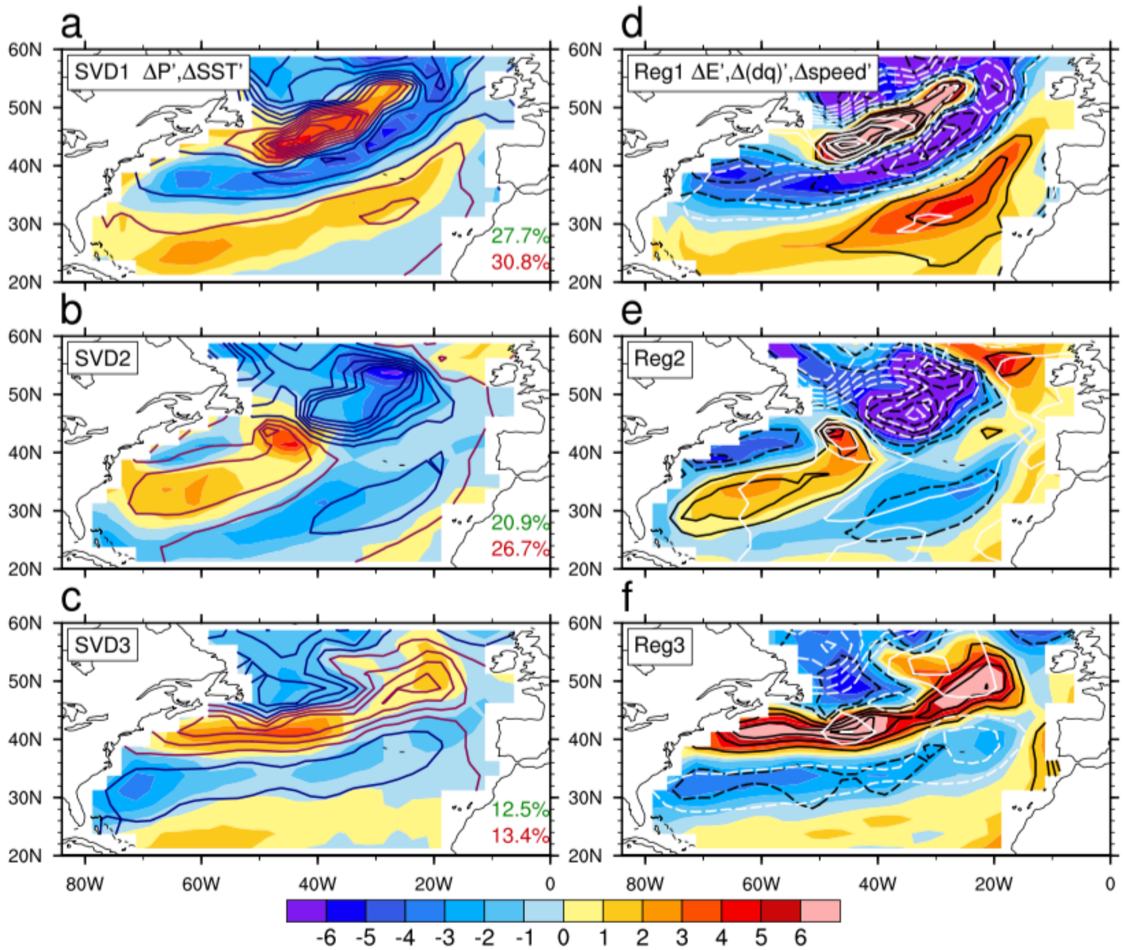


**Fig. 2.** (Left panels) First three modes of inter-model SVD between $\Delta P'$ (color shaded) and $\Delta SST'$ (contours, CI = 0.05°C) in RCP4.5 run. The explained variances for $\Delta P'$ (green letters) and $\Delta SST'$ (red) are marked at the bottom right of each panel. (Right panels) Corresponding regressions of $\Delta E'$ (color shaded), sea-air humidity gradient change [$\Delta(dq)'$, black contours, CI = 0.03g/kg] and surface wind speed change ($\Delta speed'$, white contours, CI = 0.02m/s). Zero contours omitted for clarity. The prime indicates deviation from the ensemble-mean change.

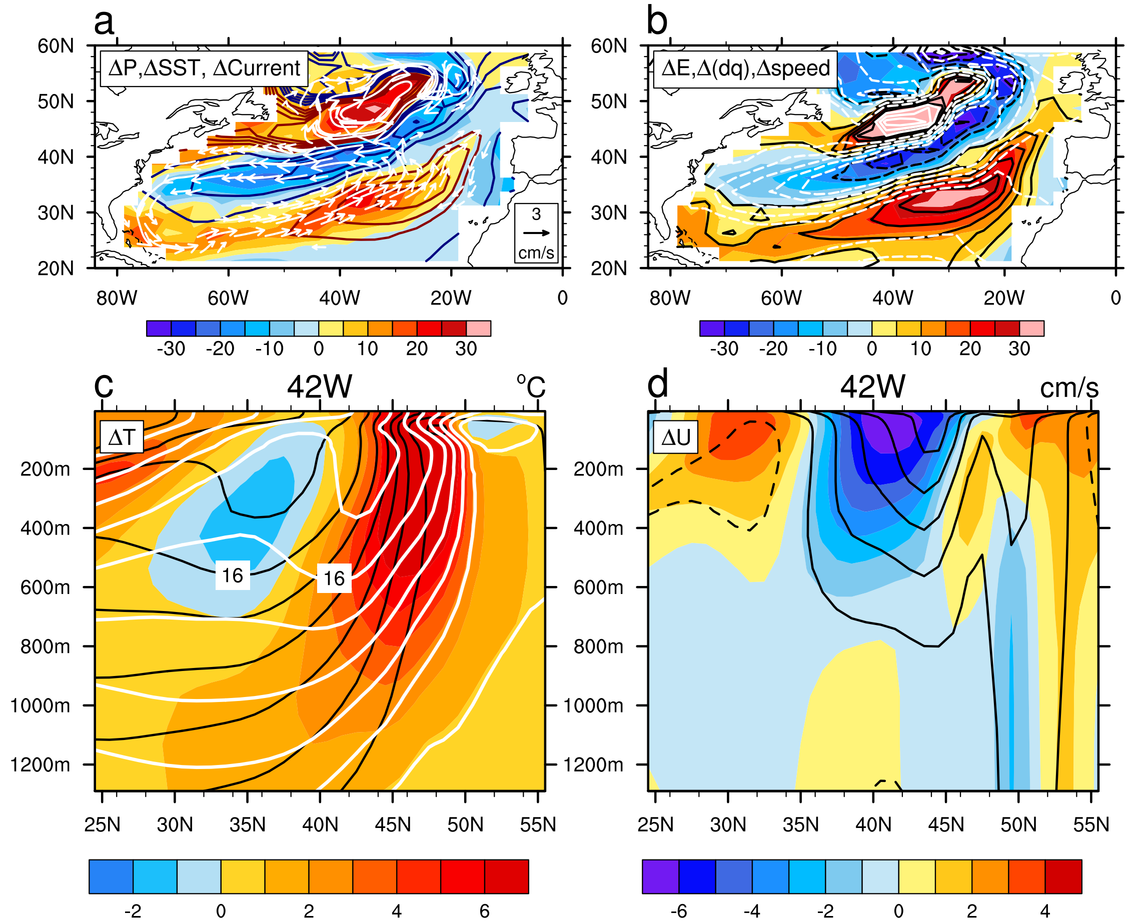


**Fig. 3.** (a) ΔP (color shaded, mm/month), ΔSST (contours, °C) and upper 50m ocean current change (vectors, cm/s); (b) ΔE (color shaded, mm/month), sea-air humidity gradient change [black contours, CI = 0.2g/kg] and surface wind speed change (white contours, CI = 0.1m/s)) in ACCESS1-0 RCP4.5 run. Vectors smaller than 1.5cm/s are omitted for clarity. Vertical transection along 42°W of present (black contours) and future (white contours) climatologies, and future-present difference (color shaded): (c) seawater temperature (°C) and (d) zonal velocity (cm/s). CI = 2°C for temperature and 2cm/s for zonal velocity.

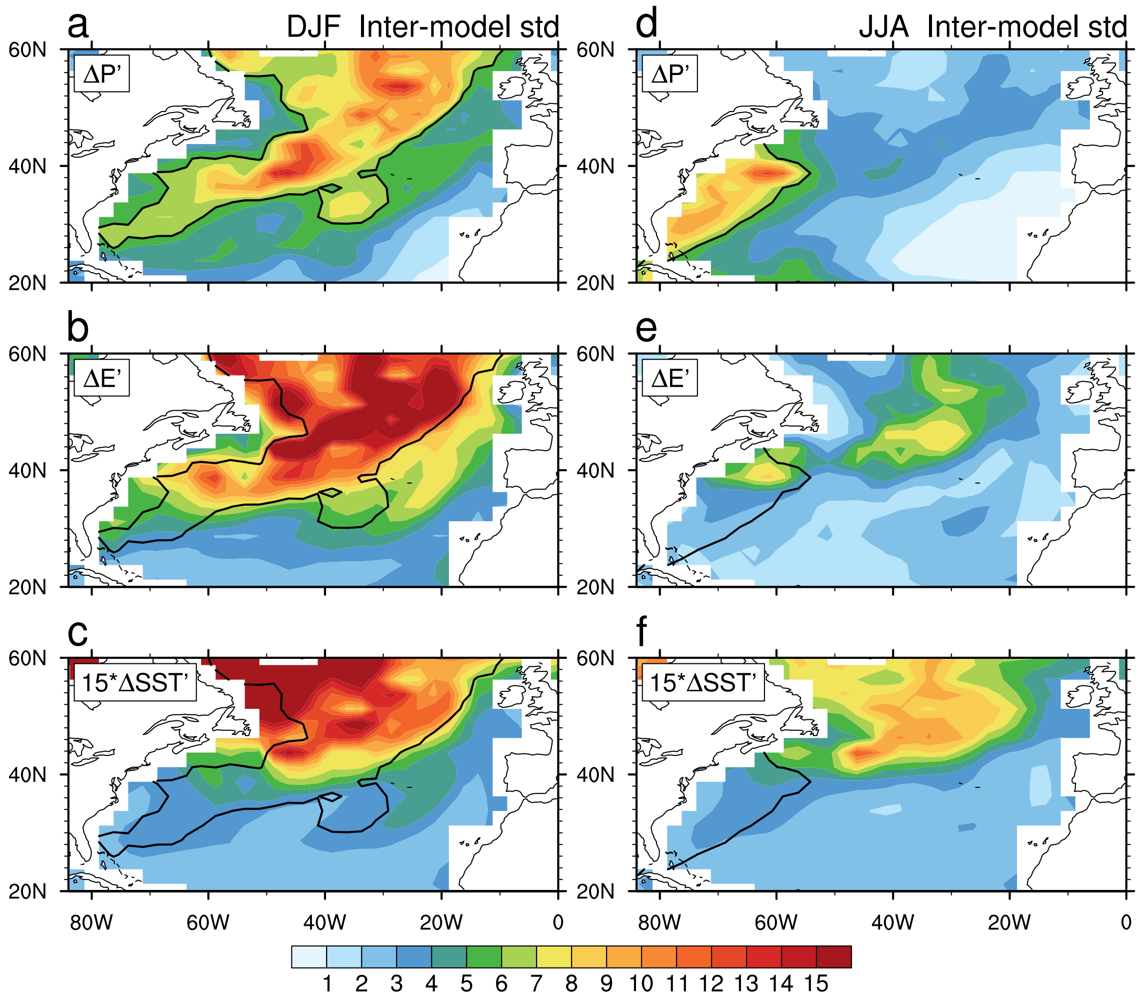


**Fig. 4.** Inter-model standard deviations of future projections in DJF and JJA, colors shaded are ΔP′ (mm/month) in (a and d), ΔE′ (mm/month) in (b and e) and ΔSST′ (°C) in (c and f). Black contours indicate value at 6 mm/month in panel (a).